Issues Concerning the Oxidation of Ni(Pt)Ti Shape Memory Alloys

J. L. Smialek[a]

[a] Structures and Materials, NASA Glenn Research Center, Cleveland, OH, 44135, USA

The oxidation behavior of the Ni-30Pt-50Ti high temperature shape memory alloy is compared to that of conventional NiTi nitinol SMAs. The oxidation rates were ~1/4 those of NiTi under identical conditions. Ni-Ti-X SMAs are dominated by TiO_2 scales, but, in some cases, the activation energy diverges for unexplained reasons. Typically, islands of metallic Ni or Pt(Ni) particles are embedded in lower scale layers due to rapid selective growth of TiO_2 and low oxygen potential within the scale. The blocking effect of Pt-rich particles and lower diffusivity of Pt-rich depletion zones are proposed to account for the reduction in oxidation rates.

Introduction

High Temperature Shape Memory Alloys have been studied for actuators in various aero-engine applications [1]. For example, ternary alloys based on the Ni-Pt-Ti system are capable of shape memory behavior under stress at temperatures in the range of 300-400^{o}C [2,3]. Oxidation effects may be expected at high temperatures and this became the focus of a number of our studies [4,5]. Basically the isothermal oxidation behavior of Ni-30Pt-50Ti was examined over 500°-900°C by TGA, SEM/EDS and XRD. It was compared to results similarly obtained for a commercial Ni-49Ti SMA. The pertinent findings can be found in [4,5], with further details in preliminary NASA Technical Memoranda. A number of interesting points of discussion arose concerning rate changes, activation energies, 'cermet' scales, and depletion zones. The purpose of the present paper is to highlight and discuss these interesting aspects in this special R.A. Rapp Honorary High Temperature Corrosion and Materials Chemistry Symposium.

Experimental

The experimental details pertaining to this discussion have been related in the prior papers [4,5]. Briefly, the oxidation kinetics of rectangular coupons of Ni-49Ti and Ni-30Pt-50Ti (at. %) were measured in dry air isothermal TGA tests, at 500-900°C for up to 100 hr. The scales were examined in plan by SEM/EDS and XRD. Duplicate 700°C samples were subjected to more detailed analyses. Serial polishing with XRD was performed on one sample to provide phase identification through the various thick oxidation layers. The companion sample was mounted and polished in cross section to provide detailed SEM/EDS characterization of features corresponding to those identified by XRD.

Results and Discussion

Oxidation Kinetics

The thermogravimetric curves for the two alloys were analyzed in great detail [4]. Basically, all the data indicated essentially parabolic behavior in log-log and parabolic plots. There were often slight deviations for early and later stage rates, yielding $k_{p,initial}$ and $k_{p,final}$. These were taken into account when presenting average values on an Arrhenius plot, figure 1. It is further determined that the rates for the Ni-30Pt-50Ti alloy were about ¼ those of the Ni-49Ti alloy on average. The activation energy for both alloys was ~250 kJ/mole. The rate constants are compared with the those produced by oxidation of pure Ti (219 kJ/mole) and pure Ni (112 kJ/mole) and appear to be most consistent with TiO_2 rates. In general, the rates of TiO_2 scale growth exceed that of NiO, except perhaps at very low temperatures. Some anomalously high rates occurred at 500°C for the Ni-49Ti alloy. The reason for this is not readily apparent, but may be associated with the observation of some $NiTiO_3$ at that temperature. It is also noted that the oxidation rates of the SMA alloys are nearly 5 orders of magnitude higher than those measured for protective α-Al_2O_3 growth on $TiAl_3$ alloys [7].

Further comparisons are shown in figure 2 for a number of studies on NiTi SMA [8-12]. Here the combined data is seen to fall within a general band, however there are divergences apparent with regard to activation energies. These are displayed as two groups consistent with either ~240 or ~140 kJ/mole. It is recalled that the former appeared to be more consistent with TiO_2 growth, while the latter is closer to that measured for NiO scales. Since all of these studies report primarily TiO_2 scales, there is no obvious explanation for the difference. Lesser amounts of $NiTiO_3$ and NiO have been detected, with tentative indications of TiO_2 anatase and TiO at low temperatures and times. The specifics for each study are summarized in Table 1, showing no apparent correlation with alloy variations or test duration.

Table I. Summary of Ni-Ti-X Oxidation Kinetics

	$k_p = A \exp(-Q/RT)$		Q					
alloy, at.%	**A (mg^2/cm^4hr)**	**A′ (g^2/cm^4s)**	**(kJ/mole)**	**(°C)**	**(hr)**	**r^2**	**reference**	
Ni30Pt50Ti	1.54×10^{12}	4.29×10^{2}	**250**	500-900	100	0.98	this study	air
Ni49Ti	6.39×10^{12}	1.78×10^{3}	**249**	600-900	100	1.00	this study	air
Ni49Ti	3.46×10^{12}	9.61×10^{2}	**259**	750-950	60	0.99	Satow (1974)	air
Ni50Ti	4.85×10^{10}	1.35×10^{1}	**225**	700-1000	6	0.96	Chu (1996)	air
Ni51Ti	1.92×10^{6}	5.33×10^{-4}	136	450-750	4	1.00	Xu (2004)	O_2
Ni49Ti	7.31×10^{6}	2.03×10^{-3}	152	530-650	4	0.96	Vojtêch (2008)	air
Ni50Ti10Cu	1.61×10^{7}	4.47×10^{-3}	143	700-925	6	1.00	Lin (2009)	air

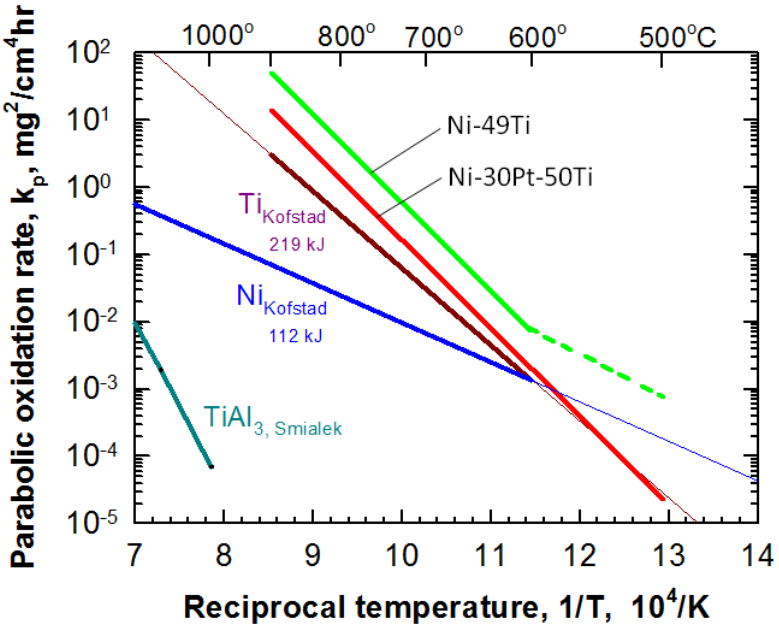

Figure 1. Arrhenius plot comparing parabolic oxidation rates for NiTi and NiPtTi shape memory alloys to TiO_2 growth on Ti, NiO growth on Ni and Al_2O_3 growth on $TiAl_3$ [4-7].

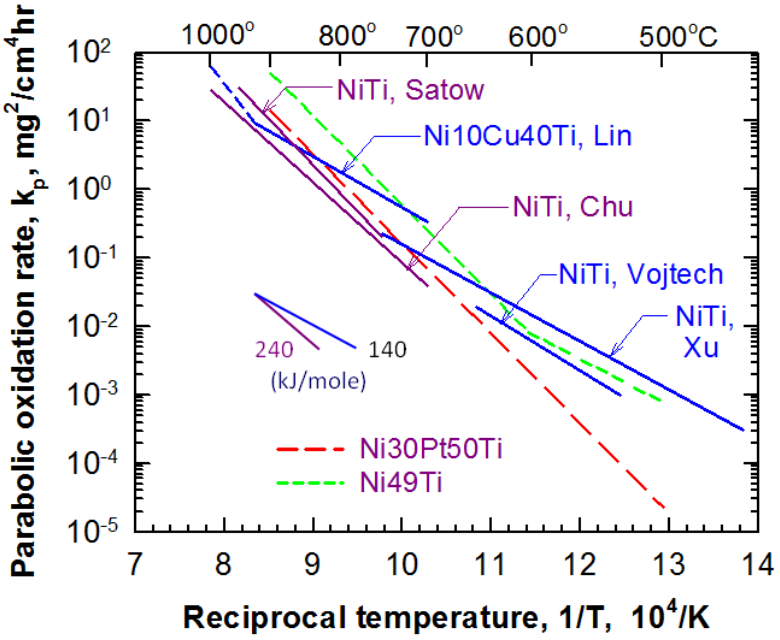

Figure 2. Arrhenius plot comparing parabolic oxidation rates of Ni-Ti-X shape memory alloys, suggesting bimodal activation energies for some systems [8-12].

Scale Morphology and Structures

The make-up of the scales has been carefully documented by SEM/EDS and XRD diffractometer scans. These characterizations were performed on the plan surface for samples tested at the various temperatures. However, occasional spalling and complex layering of the scales diluted the import of this survey. Some of the more distinctive findings were colonies of striated, outward growing, crystallographically faceted TiO_2 grains. While relatively uniform on the Ni-49Ti alloy, there was a bimodal distribution on the Ni-30Pt-50Ti alloy, with the fine grains an order of magnitude smaller, figure 3. The fine grains were occasionally the location of a few Ni (or Pt)-rich areas or particles. Spalling to inner regions of the scales revealed more of the same in a matrix of TiO_2, including Fe(Ni)-rich particles in the case of the Ni-49Ti alloy.

To complement these findings, a detailed cross-sectional study was performed, coupled with serial or taper section XRD analyses of the various layers. Duplicate samples from the middle of the test temperature range (700°C) were employed for this investigation. The cross-section for the Ni-49Ti alloy is shown in figure 4**,** labeled by the characterizations concluded from the joint SEM/EDS/XRD studies. The salient features are an outer layer of TiO_2 rutile, a thin interface with Fe_3O_4 crystals and $NiTiO_3$, a second inward growing TiO_2 rutile layer with dispersed metallic Ni particles, a roughened $D0_{24}$ Ni_3Ti depletion zone, and finally the B2 NiTi matrix.

Similarly the structures for the Ni30Pt-50Ti alloy are presented in figure 5. Here we obtain an outer scale layer composed of NiO, $NiTiO_3$, and TiO_2 rutile (light gray, medium gray, and dark gray, respectively), starting from the outermost layer. Next is the second TiO_2 rutile layer with dispersed metallic A1 Pt(Ni) particles, followed by Pt-rich stringers attached to a nearly continuous Pt-rich depletion layer. A second depletion zone of gray $L1_2$ $(Pt,Ni)_3Ti$ is encountered, with some Widmanstatten-like morphology. A new light hexagonal "$D0_{19}$" phase is finely intermingled with the $(Pt,Ni)_3Ti$, but more prevalent as a "grain boundary necklace" further into the alloy (not shown here). The remaining structures in this micrograph are dark TiC precipitates and light gray Ni(Pt)Ti B19 martensite (as-received substrate phases).

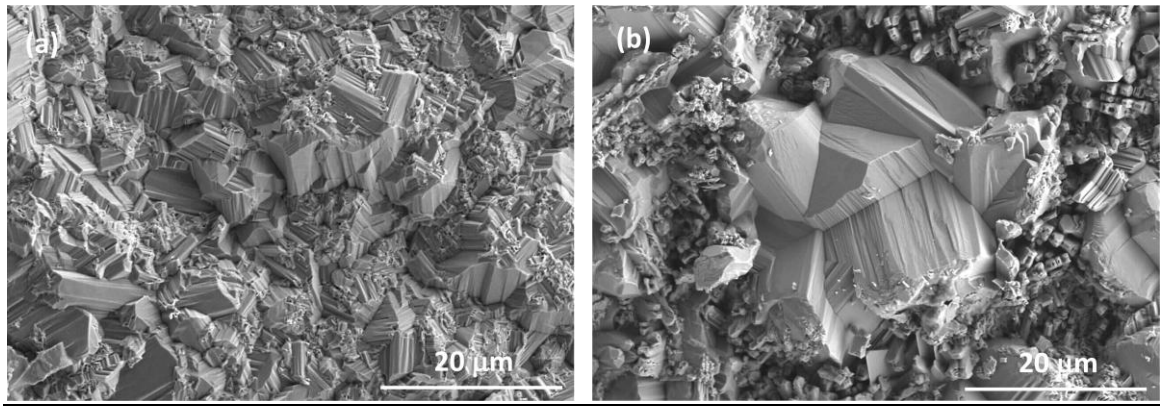

Figure 3. Faceted TiO_2 crystals formed on a) Ni-49Ti and b) Ni-30Pt-50Ti after oxidation at 800°C for 100 hr and 900°C for 10 hr, respectively.

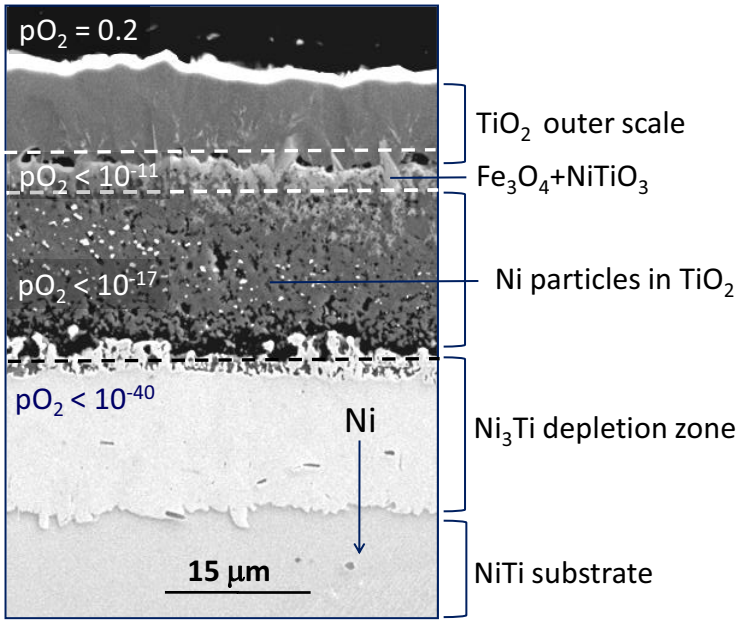

Figure 4. Cross-section of Ni-49Ti oxidized at 700°C for 100 h showing multiple scale and depletion zone layers with notional oxygen potentials.

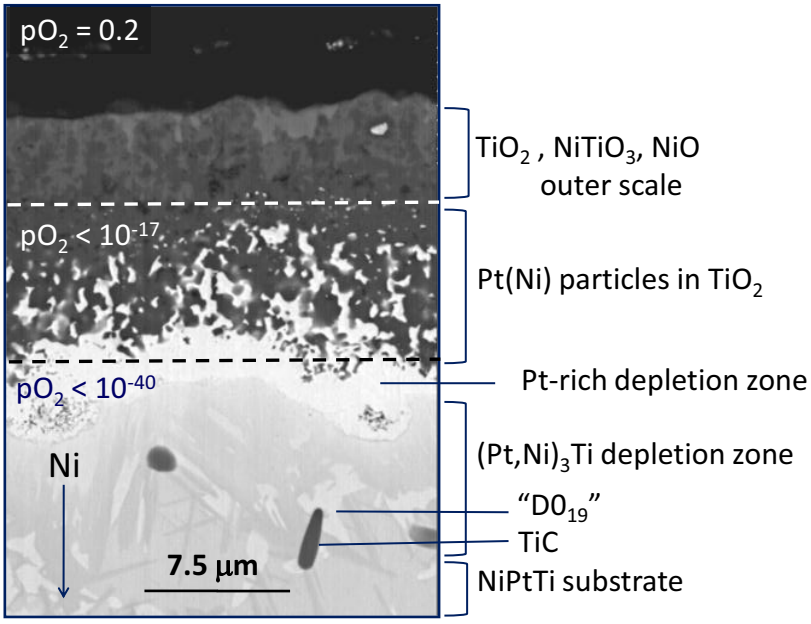

Figure 5. Cross-section of Ni-30Pt-50Ti oxidized at 700°C for 100 h showing multiple scale and depletion zone layers with notional oxygen potentials.

Mechanistic Discussion

A simplified Ellingham diagram of oxide phase stabilities vs temperature is presented in figure 6, including a nomagraph of equilibrium oxygen pressure for the oxidation of pure metals (adapted from Swalin [13]). First it is seen that the 700°C equilibrium for Fe_2O_3/Fe_3O_4 is fixed at a pO_2 of about 10^{-11} atm. Thus the NiTi scale layers at and below this interface region in figure 4 are expected to be below this oxygen potential. Outer layers are expected to be at higher pO_2. Thus it is consistent that Ni be present as oxides above this interface. Conversely, the unoxidized Ni particles in the second rutile layer correspond to a pO_2 of about 10^{-17} atm. or below. Finally the retention of Ti metal in the Ni_3Ti depletion zone would indicate a pO_2 of about 10^{-40} atm. This exercise helps provide a perspective of the oxygen potential gradient across the scale, even though this rough approximation assumed unit activity of the metal reactants. It presents a possible situation allowing for oxidized Ni phases in the outer scale layers, with metallic Ni retained in the lower scale layers.

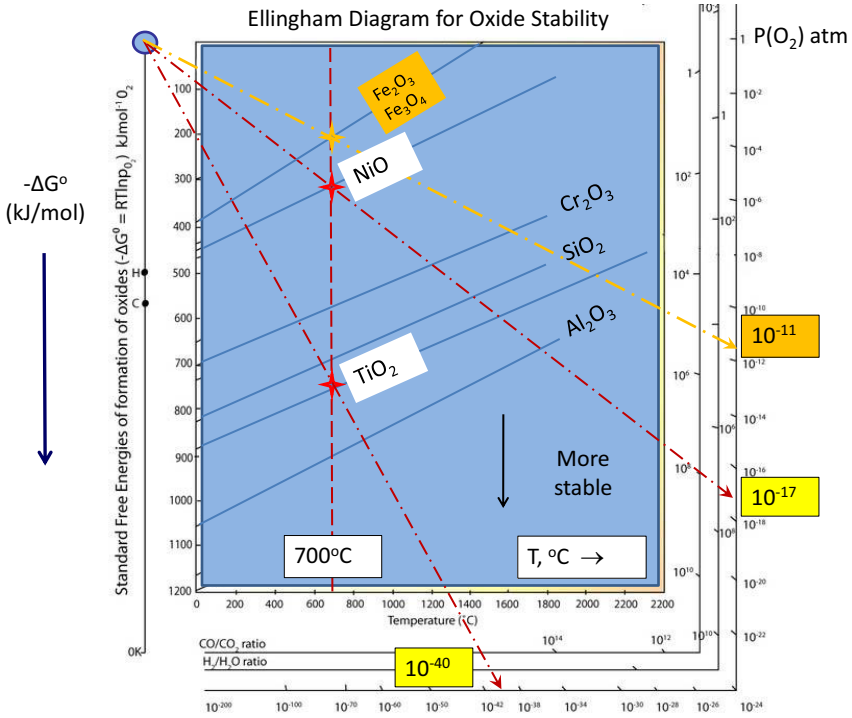

Figure 6. Simplified Ellingham/Richardson diagram showing relative 700°C oxide stabilities and corresponding $p(O_2)$ for Fe_2O_3/Fe_3O_4, Ni/NiO, and Ti/TiO_2 equilibrium (at unit activities; modified from Swalin [13]) .

Similarly, the outer layers of the scale formed on Ni(Pt)Ti are expected to be above 10^{-11} atm. and favor Ni oxidation to NiO or $NiTiO_3$ as shown in figure 5. The inner region containing metallic Ni (in solution with Pt) fixes a lower pO_2 of about 10^{-17}, while the Ti-containing $(Pt,Ni)_3Ti$ depletion zone will again be at 10^{-40} atm or below.

Kinetic factors may also play a role here as the growth rate and diffusion in TiO_2 scales are expected to be about an order of magnitude greater than those for NiO at 700°C. Accordingly, Ti denudation from the alloy and scale thickening by TiO_2 growth may be so fast that any remnant Ni is left behind unoxidized in the lower layers. To some extent,

the metallic Ni and Pt dispersed particles can be viewed as markers retained in an inward growing scale. In effect, a metastable steady state equilibrium may be reached where any incoming oxygen is totally gettered by Ti, with Ni back diffusing through the depletion zone or trapped as metallic islands in the inner oxide.

To this end, one might visualize undulations or depressions in the initial interface, possibly aggravated by oxygen in solution and a tendency for internal oxidation of Ti. In these local regions, the Ti has been depleted from the alloy, setting up a diffusive flux of Ti toward the depression. With continued oxidation, an irregular oxide-metal interface develops, advancing at the depression and leaving behind Ti-denuded fingers of alloy. These are then pinched off and isolated within the growing scale. At this point, Ostwald ripening would be expected to drive for large spherical metalloids, however a dispersion of refined spherical particles is found above the interface. Thus some aspect of solution/re-precipitation of Ni (Pt?) diffusion through TiO_2 is implied.

Pt Effects

The oxidation rate and scale thickness clearly show that Pt in the alloy has reduced the growth rate of the TiO_2 scales. Since there is no oxidation state of Pt, no argument can be made from the standpoint of ionic diffusion effects of dopants in the oxide. One consideration is simply morphological, the area fraction of Pt-rich metallic dispersions in the scale simply restrict the available area for diffusional flux through the scale [14]. Other considerations may also apply, since these Pt-rich islands or fingers represent a mature morphology that may not have been present throughout the initial oxidation process. Here one may turn to some mechanistic papers of Wagner discussing oxidation of base-noble Ni-Pt metal alloys [15], a reduction in growth rate with noble metal content due to decreasing ability to supply base metal to the growing scale.

Recently that model was critically examined by Danielewski, et al., in light of their new comprehensive data set for Ni-Pt alloys. This study obtained k_p over a wide range of Pt content, temperatures, and $p(O_2)$ [16]. Fundamental mechanistic insights were obtained from activation energy and $p(O_2)$ dependence on Pt content. Some results have been highlighted in the construction of Figure 7. Here the 1100°C k_p is seen to decrease as a function of Pt content, shown here for two extremes of $p(O_2)$. The highest k_p, i.e., for Ni-rich alloys, depends on $p(O_2)^{1/6}$, as would be expected for a defective $Ni_{1-y}O$ p-type scale dependent on $[V_{Ni}^{''}]$. In addition, these alloys exhibit a temperature dependence resulting in an activation energy of 232 kJ/mol. This value is in agreement with that for pure Ni oxidation at 228 kJ/mol. In contrast, the Pt-rich alloys show no $p(O_2)$ effect and produce an activation energy of 275 kJ/mol. The latter is similar to that found for diffusion in the alloy, 280 kJ/mol. Thus k_p reductions at high Pt contents due to an inability to supply Ni from the alloy at a rate commensurate with Ni diffusion in the scale. But it is noteworthy that there are also substantial reductions in k_p at lower Pt contents, where rate control is still due to diffusion within the scale.

Some of these findings may be applied in concept to Ni(Pt)Ti oxidation, but with reservation. The most important difference is the formation of TiO_2 scales as opposed to NiO. The former entail much faster rates and probably require higher diffusivity within the alloy to sustain scale growth. The binary alloy has 0% Pt while the HT-SMA contains 30%. The NiPtTi alloy increases to near 90% in the subsequent depletion zones. Thus trends in scale growth, expected from the Ni-Pt alloys, follow along the Pt composition in Figure 7. The drop in NiO growth rate achieved from 0 to 30% is a factor of 3.8 or a reduction to about ¼ the rate for pure Ni. This, fortuitously, is the same

reduction observed for TiO_2 growth rates between the present Ni-49Ti and Ni-30Pt-50Ti alloys. A further reduction in scale growth rate over two orders of magnitude can be associated with the extreme alloy depletion observed in the present study (second arrow in Figure 7).

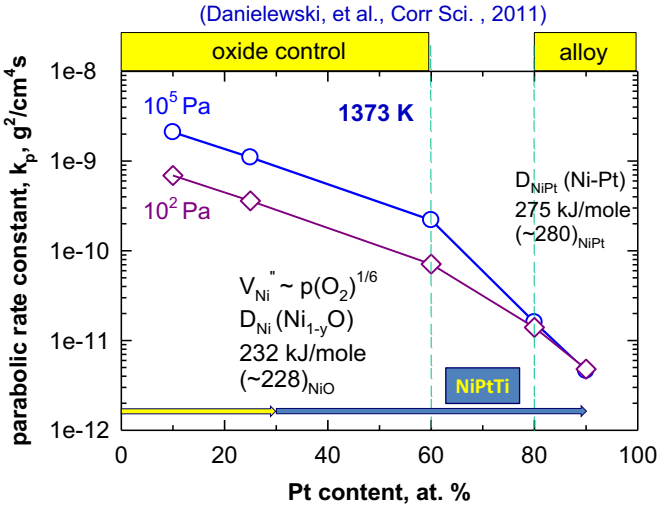

Figure 7. Effect of Pt content and $p(O_2)$ on the 1100°C parabolic oxidation rate (log scale) and activation energy for Ni-Pt alloys (after Danielewski, et al. [16]). Lower bar: superimposed Pt content of Ni-Pt-Ti SMA and depletion zones.

Concluding Remarks

The previous discussion has highlighted some of the interesting features that arose in our studies of Ni-Pt-Ti HT-SMA oxidation. The oxidation behavior most typically followed parabolic kinetics, with slight deviations. The activation energy was 250 kJ/mol, in general agreement with that observed for pure TiO_2 scales and many other NiTi SMA studies. The occasional 140 kJ/mol must be some manifestation, albeit inconsistent and unexplained, of a Ni effect. Standard surface characterization by SEM/EDS and XRD provided useful information, but was often incomplete for these relatively thick or spalled scales. To this end, duplicate cross-section and serial XRD samples were needed to identify all the layered features, even producing a semi-quantitative depth profile of scale phases and Ti-depletion zones. The outer TiO_2 scale layers contained small amounts of NiO or $NiTiO_3$, thought to be remnants of initial transient oxidation. Inner layers having an Fe_3O_4 or Ni, Pt(Ni) particles are physical evidence of a reduced $p(O_2)$ level within the thick multilayer scales. At some point a heavy buildup of Pt-rich metal, as islands or a continuous depletion zone, can be considered a diffusion limiting factor in the growth of TiO_2 scales, as discussed in light of model Ni-Pt alloys.

Acknowledgments

The contributions of D. Humphrey, A. Garg, R. Rogers, R. Garlick, R. Noebe, and J. Buehler in these HT-SMA oxidation studies are gratefully acknowledged. (Funded by NASA Fundamental Aeronautics/Supersonics; Dr. Dale Hopkins, API).

References

1. J. Ma, I. Karaman, and R.D. Noebe, *Int. Mater. Rev.*, **55**, 257 (2010).
2. R. Noebe, D. Gaydosh, S. Padula, A. Garg, T. Biles, and M. Nathal, *Proc. SPIE*, **5761**, 364 (2005).
3. S. Padula, G. Bigelow, R. Noebe, and D. Gaydosh, and A. Garg, *SMST 2006: Proceedings of the International Conference on Shape Memory and Superelastic Technologies,* ASM International, Metals Park, OH., 787 (2008).
4. J.L. Smialek, D.L. Humphrey, and R.D. Noebe, *Oxid. Met.*, **74**, 125 (2010); also NASA TM-2007-214697.
5. J.L. Smialek, A. Garg, R.B. Rogers and R.D. Noebe, *Oxide Scales Formed on NiTi and NiPtTi Shape Memory Alloys,* NASA/TM–2011-217096. (also *Metall. Trans.,* in press).
6. P. Kofstad, *High Temperature Corrosion*, Elsevier Applied Science, London, pp. 212 and 293 (1988).
7. J.L. Smialek and D.L. Humphrey, *Scripta Met. et Mat*., **26**, 1763 (1992).
8. T. Satow, T. Isano, and T. Honma, *J. Jn. Inst. Met.,* **38**, 242 (1974).
9. C.L. Chu, S.K. Wu, Y.C. Yen, *Mater. Sci. Eng. A*, **216**, 193 (1996).
10. C.H. Xu, X.Q. Ma, S.Q. Shi and C.H. Woo, *Mater. Sci. Eng., A*, **371**, 45 (2004).
11. D. Vojtěch, P. Novák, M. Novák, L. Jaska, T. Fabián, J. Maixner and V. Machovič, *Intermetallics*, **16**, 424 (2008).
12. K-N. Lin and S-K Wu, *Oxid. Met.,* **71**, 187 (2009).
13. R.A. Swalin, *Thermodynamics of Solids*, p. 84 (1964).
14. R.A. Rapp, private communication, this conference (2011).
15. C. Wagner, *Atom Movemements*, ASM, Cleveland, OH, 153 (1951).
16. M. Danielewski, Z. Grzesik, and S. Mrowec, *Corr. Sci.*, **53**, 2785 (2011).